ECS Solid State Letters, **2** (8) P63-P65 (2013)
2162-8742/2013/2(8)/P63/3/$31.00 © The Electrochemical Society

Improved Resistive Switching Characteristics by Al_2O_3 Layers Inclusion in HfO_2-Based RRAM Devices

Chun-Yang Huang,[a] Jheng-Hong Jieng,[a] Wen-Yueh Jang,[b] Chen-Hsi Lin,[b] and Tseung-Yuen Tseng[a,z]

[a]*Department of Electronics Engineering and Institute of Electronics, National Chiao Tung University, Hsinchu 30010, Taiwan*
[b]*Winbond Electronics Corporation, Hsinchu 30010, Taiwan*

A series of complex HfO_2/Al_2O_3 layer by layer resistive random access memory(RRAM) structure grown by atomic layer deposition are investigated. The modulation of forming voltage can be achieved by controlling the number of Al_2O_3 layers in HfO_2 devices. In addition, the crystallization temperature of HfO_2 based RRAM devices can also be improved by insetting Al_2O_3 layers in HfO_2 film. Compared with pure HfO_2 device, a significant improvement in resistive switching properties such as forming voltage variation and the distribution of HRS/LRS during resistance switching is demonstrated in the HfO_2/Al_2O_3 layer by layer devices. Moreover, good endurance characteristic and highly reliable multibit operation are also achieved in this device structure.
 [DOI: 10.1149/2.006308ssl]

Manuscript submitted April 15, 2013; revised manuscript received May 20, 2013. Published May 31, 2013.

Resistive random access memory (RRAM) is a promising candidate to replace the currently flash memory device due to its simple structure, low voltage operation, high scalability, and multibit data storage.[1,2] It is found that transition metal oxides (TMOs) can be utilized in RRAM devices, such as ZrO_2,[3,4] NiO,[5] and HfO_2.[6–11] Among those various TMOs, HfO_2 is one of the appealing materials that had considerable attention owing to its high dielectric constant (k), superior resistive switching (RS) performance, and compatible standard complementary metal oxide semiconductor (CMOS) technology process.[6] However, the thermal stability of HfO_2 thin film is a serious issue for memory characteristics due to the low crystallization temperature (<400°C).[12] The RRAM devices with crystalline phase HfO_2 film suffer the RS behaviors variation due to location dependent conductive filament (CF) formation. For example, if CF grows along the grain boundaries of polycrystalline HfO_2 film, low forming voltage and good RS behaviors are observed, whereas high forming voltage is detected in amorphous phase and crystalline phase HfO_2 RRAM devices.[7] On the other hand, crystalline phase HfO_2 film, which is stoichiometric structure, prevents creating enough oxygen vacancies in RRAM devices for RS behaviors.[8] Moreover, the high forming voltage crystalline phase HfO_2 film may cause RRAM devices hard breakdown during forming process. Besides, for the scaled RRAM devices, the larger non-uniformity grain boundaries for cell by cell with crystalline phase HfO_2 film will cause the variation of device performance.[9] Therefore, the amorphous phase HfO_2 exhibiting uniformity film quality is suitable for RRAM development. According to previous literature, the RS behaviors are dependent on the degree of crystalline of HfO_2 film, which critically influences the device yield. Hence, this phenomenon of low crystallization temperature in HfO_2 is not allowed existence in further RRAM applications.

In this letter, we fabricate Hf_xAl_yO films, which are the architecture with a series of complex HfO_2/Al_2O_3 layer by layer structure by using atomic layer deposition system (ALD), for HfO_2-based RRAM devices. Here, we show the insetting Al_2O_3 layers would significantly increase the crystallization temperature of HfO_2 film. Moreover, the forming voltage variation of HfO_2 film can be reduced by the insetting Al_2O_3 layers in the film during ALD deposition. The memory performances such as endurance, retention, and multibit storage properties are also discussed.

Experimental

The 5-nm thin HfO_2, Hf_xAl_yO, and Al_2O_3 RS layers were deposited on Pt/Ti/SiO_2/Si substrates by using ALD at 250°C and 0.2 Torr Ar ambient with $Hf[N(C_2H_5](CH_3)]_4$, $(CH_3)_3Al$, and H_2O precursors. The Hf_xAl_yO films were the t-series of complex m-cycle HfO_2 layers and n-cycle Al_2O_3 layers structure, or $\{(HfO_2)_m/(Al_2O_3)_n\}_t$ multilayer architecture. The HfO_2 layers were firstly deposited and then Al_2O_3 layers during every series deposition. For example, the 5-nm $Hf_{0.7}Al_{0.3}O$ film was composed of $t = 8$ series of mixing $m = 6$ cycles HfO_2 layers and $n = 1$ cycle Al_2O_3 layer. The material compositions of Hf_xAl_yO films were modified by different m and n values. Besides, all the films' thicknesses controlled by t values were kept in 5-nm for comparison, as listed in Table I. Subsequently, the post deposition annealing (PDA) processes were carried out for X-ray diffraction (XRD) analysis at different temperatures in N_2 ambient for 30 s. Finally, a 50-nm thick Ti top electrode and a 20-nm thick Pt capping layer with a diameter of 150 μm were deposited by electron beam evaporation. All the electrical characteristics were performed using an Agilent 4156C semiconductor parameter analyzer.

Results and Discussion

Fig. 1a reveals the crystallization temperature of Hf_xAl_yO films as a function of different Al percentage (Al% = y/[x + y]). By utilizing Al_2O_3 layer inclusion in HfO_2 film, the crystallization temperature increases with an increase of the Al content from 400°C to 1200°C. It can be explained that Al distributes uniformly in Hf_xAl_yO films and Al acts as a network modifier to suppress the crystallization of HfO_2 film. The inset of Fig. 1a shows the XRD patterns of HfO_2 and $Hf_{0.7}Al_{0.3}O$ films with as-deposited and 400°C PDA processes, respectively. The $Hf_{0.7}Al_{0.3}O$ film is still in amorphous state after 400°C PDA process. However, the HfO_2 film shows crystalline phase. Besides, due to the crystallization temperature improved by inserting Al_2O_3 layers in HfO_2 film, the as-deposited and 400°C PDA $Hf_{0.7}Al_{0.3}O$ samples both exhibit amorphous state. A typical cross-section TEM image of the amorphous Ti/$Hf_{0.7}Al_{0.3}O$/Pt RRAM device is shown in Fig. 1b.

The forming voltages (V_F) in the HfO_2 and Hf_xAl_yO RRAM devices are also dependent on Al percentage, as shown in Fig. 2a. Al incorporated in the HfO_2 devices induce the increasing of the V_F from 2.4 V for HfO_2 device to 4.1 V for Al_2O_3 device. On the other words, the V_F can be modulated by different Al percentage inclusion in HfO_2 RRAM devices. It is due to that the breakdown strength in dielectric material is dependent on $(k)^{-1/2}$.[13] Besides, the dielectric constants in Hf_xAl_yO RRAM devices are a function of Al percentage, which

Table I. Components of 5-nm $\{(HfO_2)_m/(Al_2O_3)_n\}_t$ multilayer architecture.

Composition	HfO_2	$Hf_{0.7}Al_{0.3}O$	$Hf_{0.55}Al_{0.45}O$	$Hf_{0.11}Al_{0.89}O$	Al_2O_3
m-cycle	1	6	3	1	0
n-cycle	0	1	1	3	1
t-series	56	8	14	14	53

[z]E-mail: tseng@cc.nctu.edu.tw

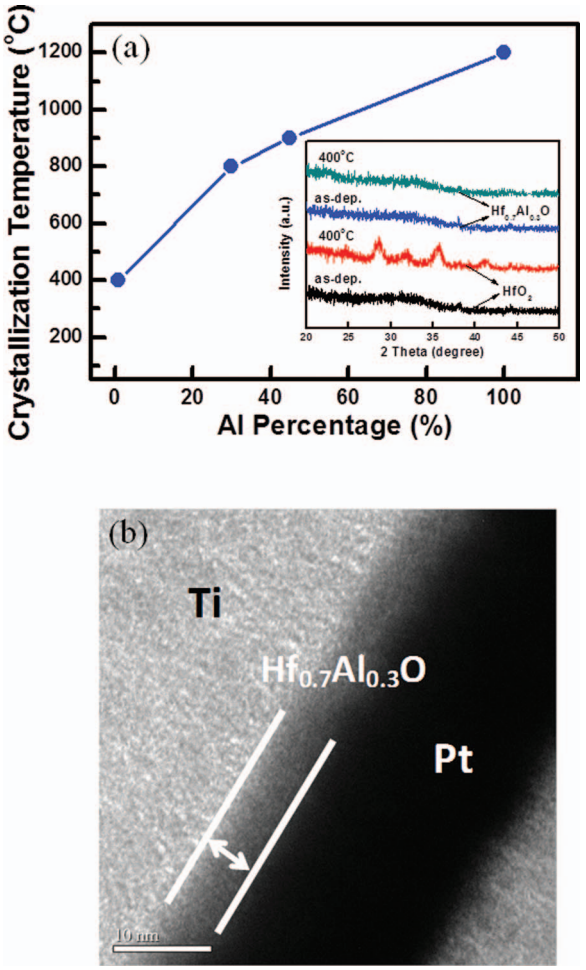

Figure 1. (a) Crystallization temperature of different Al percentage in Hf_xAl_yO films. The inset shows XRD patterns of HfO_2 and $Hf_{0.7}Al_{0.3}O$ films with as deposited and 400°C PDA, respectively. (b) Typical cross-section TEM image of the Ti/$Hf_{0.7}Al_{0.3}O$/Pt RRAM device.

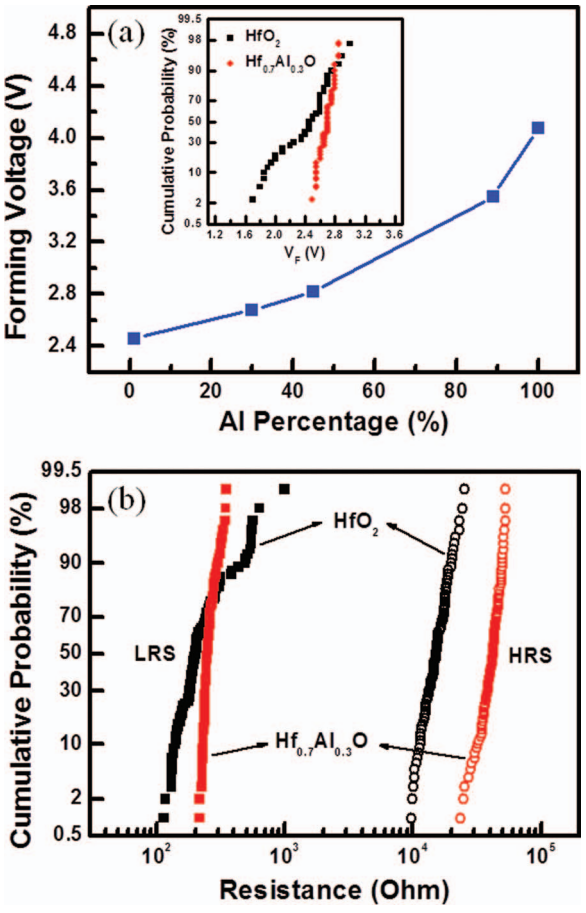

Figure 2. (a) Forming voltage of Hf_xAl_yO devices as a function of Al percentage. The inset shows the statistical distributions of forming voltages of HfO_2 and $Hf_{0.7}Al_{0.3}O$ devices. (b) Resistance distributions for 100 dc sweep cycles of HfO_2 and $Hf_{0.7}Al_{0.3}O$ devices. The resistances are measured at a read voltage of 0.3 V.

k value decreases from ~25[14] (HfO_2) to ~9[15] (Al_2O_3). Therefore, the HfO_2 device shows the smallest V_F than other Hf_xAl_yO devices. The inset of Fig. 2a shows the comparison of V_F distribution in HfO_2 device with that in $Hf_{0.7}Al_{0.3}O$ device. The $Hf_{0.7}Al_{0.3}O$ device reveals a much narrower V_F distribution than HfO_2 device. This phenomenon is due to that the oxygen vacancies are easier to generate and assemble along Al atoms from bottom to top electrodes and the CF grows stably along Al atoms in RS layer.[16] In addition, the Ti top electrode contacts with Al_2O_3 layer in $Hf_{0.7}Al_{0.3}O$ film. Comparing to HfO_2, the top thin Al_2O_3 layer can enhance the electric field due to lower dielectric constant.[17] The formation and rupture of CF can be confined stably at the thin Al_2O_3 layer. Therefore, the statistical distributions of high resistance state (HRS) and low resistance state (LRS) during resistance switching cycles are greatly improved, as shown in Fig. 2b. Table II lists the comparison of RS properties of various Hf_xAl_yO components. Obviously, the standard deviations of operation voltages in multilayer structure are smaller than pure HfO_2 and Al_2O_3 devices. Besides, the I-V RS properties of $Hf_{0.7}Al_{0.3}O$, $Hf_{0.55}Al_{0.45}O$, and $Hf_{0.11}Al_{0.89}O$ devices are almost the same(not shown here), but $Hf_{0.55}Al_{0.45}O$ and $Hf_{0.11}Al_{0.89}O$ devices have higher forming voltages with larger standard deviation. Therefore, we choose the $Hf_{0.7}Al_{0.3}O$ device for more detailed studies.

To further confirm the RS performance, the electrical properties of the $Hf_{0.7}Al_{0.3}O$ device are also studied. Fig. 3a depicts the endurance characteristic of the $Hf_{0.7}Al_{0.3}O$ device after post metal annealing at 400°C for 30 min in vacuum ambient. The resistance ratios of HRS/LRS can be well retained after more than 11000 switching cycles under set voltage (V_{set}) of 0.6 V and reset voltage (V_{reset}) of −0.5 V applied on Ti top electrode. Fig. 3b shows the read disturbance property of the $Hf_{0.7}Al_{0.3}O$ device under a positive voltage stress (0.3 V) at room temperature. It is clearly shown that both HRS and LRS do not exhibit any degradation for more than 10^4 s.

According to the CF model, CF will form when a set voltage applied on the device.[18] The multistates in RRAM device are dependent on the CF size.[5,19] Therefore, the level of dissolution of CF can be achieved by different stopping voltage (V_{stop}) in the reset sweep. Hence, the multibit storage operation of the $Hf_{0.7}Al_{0.3}O$ device can be achieved by changing V_{stop}, as shown in Fig. 4a. In addition, to

Table II. Resistive switching characteristics of different components of Hf_xAl_yO devices. μ is the mean value and σ is the standard deviation.

Composition	HfO_2	$Hf_{0.7}Al_{0.3}O$	$Hf_{0.55}Al_{0.45}O$	$Hf_{0.11}Al_{0.89}O$	Al_2O_3
V_F (μ/σ)	2.42 / 0.34	2.69 / 0.09	2.78 / 0.16	3.51 / 0.16	4.09 / 0.24
V_{set} (μ/σ)	0.92 / 0.11	0.69 / 0.03	0.99 / 0.05	0.75 / 0.05	1.25 / 0.21
$\lvert V_{reset}\rvert$ (μ/σ)	0.65 / 0.08	0.52 / 0.04	0.77 / 0.09	0.58 / 0.04	0.62 / 0.07

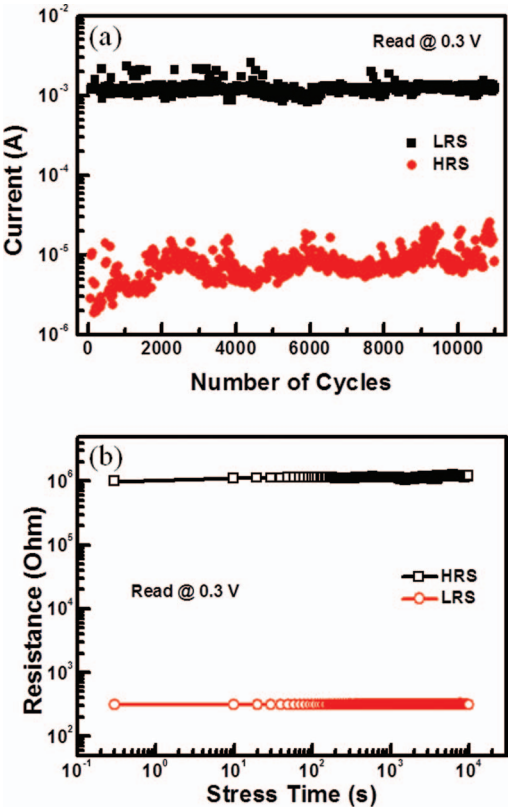

Figure 3 (a) Endurance characteristic of $Hf_{0.7}Al_{0.3}O$ device for 11000 switching cycles. (b) Read disturbance behavior for the device at room temperature.

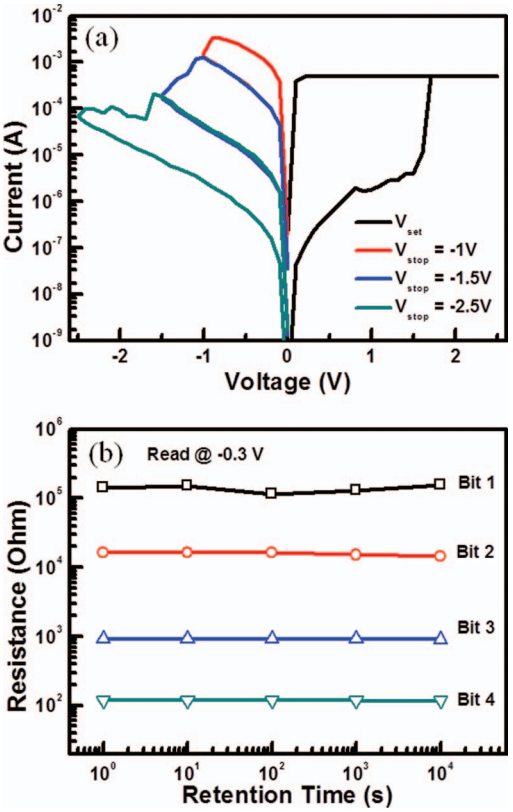

Figure 4 (a) Multibit characteristic obtained by different V_{stop} value. (b) Retention characteristic of multibit storage states of $Hf_{0.7}Al_{0.3}O$ device at room temperature.

clearly identify the different states of multibit storages in nonvolatile memory application, the interval of each storage state should be large enough (∼10 times) to detect by operation system. Therefore, the resistance state of bit 1 or on state is achieved by V_{set} at 1 mA compliance current, and the other off states from bit 2 to bit 4 are achieved by changing V_{stop} from −1 V to −1.5 V and −2.5 V, respectively. Fig. 4b demonstrates the retention measurement of multibit storages of the $Hf_{0.7}Al_{0.3}O$ device with a read voltage of 0.3 V for memory performance. All bits of storage are almost kept at the same resistance values without observable degradation after 10^4 s. Based on above results, the $Hf_{0.7}Al_{0.3}O$ device exhibits more stable and uniform RS characteristics than pure HfO_2 device.

Conclusions

The thermal stability can be improved by inserting Al_2O_3 layers in HfO_2 film. Base on experimental results, the crystallization temperature and forming voltage of HfO_2 based RRAM devices can be modulated by changing the number of Al_2O_3 layers in HfO_2 film during ALD deposition. In addition, the $Hf_{0.7}Al_{0.3}O$ device shows superior thermal stability and less variation of resistive switching operations than pure HfO_2 device. Especially, the device exhibits good memory performances, including low operation voltage, reproducible endurance, reliable read disturbance, and multibit storage characteristics. Above results suggest that the $Hf_{0.7}Al_{0.3}O$ device is promising for next generation nonvolatile memory application.

Acknowledgment

This work is supported by National Science Council, Taiwan, under Project No. NSC 99-2221-E-009-166 - MY3.

References

1. R. Waser, R. Dittmann, G. Staiko, and K. Szot, *Adv. Mater.*, **21**, 2632 (2009).
2. J. J. Yang, D. B. Strukov, and D. R. Stewart, *Nat. Nanotechnol.*, **8**, 13 (2013).
3. M. C. Wu, Y. W. Lin, W. Y. Jang, C. H. Lin, and T. Y. Tseng, *IEEE Electron Device Lett.*, **32**, 1026 (2011).
4. C. Y. Lin, C. Y. Wu, C. Y. Wu, T. C. Lee, F. L. Yang, C. Hu, and T. Y. Tseng, *IEEE Electron Device Lett.*, **28**, 366 (2007).
5. D. Ielmini, F. Nardi, C. Cagli, and A. L. Lacaita, in *Proc. International Reliability Physics Symposium.*, 5D.1.1 (2010).
6. H. Y. Lee, P. S. Chen, T. Y. Wu, Y. S. Chen, C. C. Wang, P. J. Tzeng, C. H. Lin, F. Chen, C. H. Lien, and M. J. Tsai, *Tech Dig Int Electron Device Meet.*, 297 (2008).
7. M. Lanza, G. Bersuker, M. Porti, E. Miranda, M. Nafria, and X. Aymerich, *Appl. Phys. Lett.*, **101**, 193502 (2012).
8. M. G. Sung, W. G. Kim, J. H. Yoo, S. J. Kim, J. N. Kim, B. G. Gyun, J. Y. Byun, T. W. Kim, W. Kim, M. S. Joo, J. S. Roh, and S. K. Park, in *Proc. International Reliability Physics Symposium.*, 6B.5.1 (2011).
9. B. Govoreanu, G. S. Kar, Y-Y. Chen, V. Paraschiv, S. Kubicek, A. Fantini, I. P. Radu, L. Goux, S. Clima, R. Degraeve, N. Jossart, O. Richard, T. Vandeweyer, K. Seo, P. Hendrickx, G. Pourtois, H. Bender, L. Altimime, D. J. Wouters, J. A. Kittl, and M. Jurczak, *Tech Dig Int Electron Device Meet.* 729 (2011).
10. C. Walczyk, D. Walczyk, T. Schroeder, T. Bertaud, M. Sowinska, M. Lukosius, M. Fraschke, D. Wolansky, B. Tillack, E. Miranda, and C. Wenger, *IEEE Trans. Electron Devices*, **58**, 3124 (2011).
11. Y. Y. Chen, L. Goux, S. Clima, B. Govoreanu, R. Degraeve, G. S. Kar, A. Fantini, G. Groeseneken, D. J. Wouters, and M. Jurczak, *IEEE Trans. Electron Devices*, **60**, 1114 (2013).
12. A. Salaun, H. Grampeix, J. Buckley, C. Mannequin, C. Vallee, P. Gonon, S. Jeannot, C. Gaumer, M. G. Jean, and V. Jousseaume, *Thin Solid Films*, **525**, 20 (2012).
13. J. W. McPherson, J. Kim, A. Shanware, H. Mogul, and J. Rodriguez, *IEEE Trans. Electron Devices*, **50**, 1771 (2003).
14. T. Bertaud, C. Bermond, T. Lacrevaz, C. Vallee, Y. Morand, B. Flechet, A. Farcy, M. Gros-Jean, and S. Blonkowksi, *Microelectronic Engineering*, **87**, 301 (2010).
15. K. C. Chiang, C. H. Lai, A. Chin, T. J. Wang, H. F. Chiu, J. R. Chen, S. P. McAlister, and C. C. Chi, *IEEE Electron Device Lett.*, **26**, 728 (2005).
16. S. Yu, B. Gao, H. Dai, B. Sun, L. Liu, X. Liu, R. Han, J. Kang, and B. Yu, *Electrochem. Solid-State Lett.*, **13**, H36 (2010).
17. Q. Q. Sun, J. J. Gu, L. Chen, P. Zhou, P. F. Wang, S. J. Ding, and D. W. Zhang, *IEEE Electron Device Lett.*, **32**, 1167 (2011).
18. S. Y. Wang, D. Y. Lee, T. Y. Tseng, and C. Y. Lin, *Appl. Phys. Lett.*, **95**, 112904 (2009).
19. M. C. Wu, W. Y. Jang, C. H. Lin, and T. Y. Tseng, *Semicond. Sci. Technol.*, **27**, 065010 (2012).